CHAPTER 6

Green synthesis of iron nanoparticles using plant extracts of *Abrus precatorius* and *Strychnos nux-vomica* for the removal of Cr(VI) and malachite green dye from water

Chapter 6

Green synthesis of iron nanoparticles using plant extracts of Abrus precatorius and Strychnos nux-vomica for the removal of Cr(VI) and malachite green dye from water

6.1. Introduction

Different synthesis routes were developed for Fe nanoparticles including physical, chemical and biological methods. Chemically synthesised Fe nanoparticles get easily oxidised in aerobic conditions and agglomerated due to the magnetic property of Fe nanoparticles. Researchers introduced supporting material and stabilising agents for iron nanoparticles to overcome this problem. Even though these materials decrease the agglomeration and oxidation tendency of the Fe nanoparticles, they may adversely affect the efficiency of Fe nanoparticles due to the competition for the active sites with target pollutants. The high production cost and water pollution due to residual toxic reductants are also the downsides of chemically synthesised Fe nanoparticles[1].

Green synthesis of Fe nanoparticles is a suitable alternative for chemically synthesised nanoparticles. Although plants, microorganisms and enzymes were used in green synthesis, plant extracts are the most investigated green reducing agents for Fe nanoparticles. In green synthesis, Fe nanoparticles were prepared by the simple mixing of Fe precursor solution with plant extract at room temperature. High activity, small particle size, high dispersibility, high stability, nontoxicity, cost-effectiveness and environmental friendliness are the attractive features of green Fe nanoparticles. Also, it does not require any additional supporting, stabilising or capping agents. So far, various plant extracts such as *Eucalyptus globules*, *Amaranthus dubius*, *Emblica Officinalis*, *Citrus limetta*, *Moringa oleifera*, green tea, Aloe vera and Clove have been reported for the synthesis of Fe nanoparticles. Most plant extracts are derived from plant leaves and water as the extracing solvent. The critical active components present in the plant extract for reducing Fe^{3+} ions are polyphenols, flavonoids, amino acids, terpenoids, reducing sugars, steroids, saponins, vitamins, alkaloids and organic acids. Diverse plant species and their complex bioactive components are still unknown to the world. It makes the booster on the search of the most

appropriate and strong reducing agent for Fe nanoparticles, even though some plant extracts have succeeded in the effective production of Fe nanoparticles[2].

In this study, two novel plant extracts, ethanolic seed coat extracts of *Abrus precatorius* (AP) and *Strychnos nux-vomica* (SN) were selected for the effective production of Fe nanoparticles. Photographs of seeds of AP and SN are shown in figure 6.1. AP, commonly known as rosary pea, is a leguminous plant native to India and seen in other tropical and subtropical areas. Traditionally, the leaves, seeds and roots were used for medicinal purposes[3]. Recently, zinc sulfide nanoparticles were produced from AP leaf extract and tested for toxicity using *Eudrilus eugeniae*[4]. Silver nanoparticles produced from the leaf extract of AP showed antibacterial activity against gram-positive and gram-negative bacteria[5]. The AP seeds are usually tiny and have a red and black seed coat. Campesterol, cholesterol, palmitic acid, lignoceric acid, linoleic acid, oleic acid, β-sitosterol, stigmasterol, trigonelline and brassicasterol are the significant components contained in AP seed[3]. *Strychnos nux-vomica* is a deciduous tree native to southeast Asia and belonging to the *Loganiaceae* family[6]. Its dried seeds are used to treat cancer, rheumatic pain, arthritis, inflammation and central nervous system disorders in traditional medicine[7]. Alkaloids, flavonoids, tannins, saponins and glycosides are the phytochemicals present in the SN and are responsible for its antioxidant, antidiabetic, antidiarrhoeal, antiviral, analgesic and anti-inflammatory properties[6]. SN contains two major alkaloids (strychnine and brucine) and a significant amount of glucoside (loganic acid)[8]. Other phytochemicals present in SN are α-colubrine, β-colubrine, 3-methoxyicajine, protostrychnine, novacine, n-oxystrychnine, pseudostrychnine, isostrychnine, chlorogenic acid, vomicine and igasurine[9]. In 2018, ZnO phytonano composites were prepared from aqueous leaf extract of *Strychnos nux-vomica*, exhibiting potential antimicrobial activity[10]. Rectified ethanol is used as the extracting solvent since it dissolves the majority of the plant bioactive components and prevents the growth of microbes during storage.

This work adopts a simple, eco-friendly method for synthesising Fe nanoparticles using AP and SN plant extracts to remove Cr(VI) and malachite green dye from water. In the presence of hydrogen peroxide, Fe nanoparticles act as Fenton-like catalyst and produce more hydroxyl radicals. These hydroxyl radicals can cause the degradation of the dye molecules[2,11]. The specific objectives are to 1) synthesise Fe nanoparticles using AP and SN plant extract, 2) examine the chemical reactivity of AP-Fe and SN-Fe for the

removal of Cr(VI) and malachite green dye from water, 3) investigate the influence of different parameters such as initial pollutant concentration, pH, the dosage of adsorbent and contact time during the removal of pollutant.
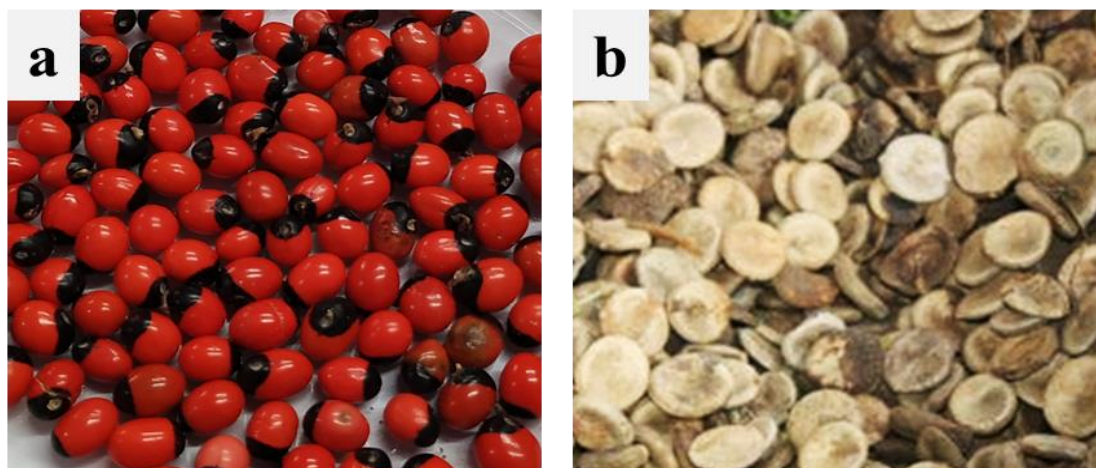
Figure 6.1 *Photographs of seeds of Abrus precatorius (a) and Strychnos nux-vomica (b)*

6.2. Experimental details

6.2.1 Preparation of plant extracts and phytogenic Fe nanoparticles

Preparation of AP and SN extract

The dried seeds of *Abrus precatorius* and *Strychnos nux-vomica* collected from the local market were washed and dried to remove impurities and moisture. AP seeds were crushed into small pieces using a pestle and mortar and seed coats were separated manually. SN seeds were cut into small pieces, ground using a mixer and feathery seed coats were collected manually. The plant extract was prepared by refluxing 4g of plant seed coat in 100 mL ethanol at a temperature of 90ºC for 2 hours. The extract was then cooled, filtered using Whatman number 41 filter paper and stored at 4ºC for further use.

Synthesis of phytogenic Fe nanoparticles

Fe nanoparticles were synthesised by mixing the prepared plant extracts with 0.01 M ferric chloride ethanol solution at a 1:1 volume ratio at room temperature. The rapid development of black colour suspension indicates the formation of Fe nanoparticles. This suspension was centrifuged and the collected nanoparticles were lyophilised and then stored in airtight vials for characterisation studies.

6.2.2   Batch experiments

Cr(VI) removal studies

To simplify the removal studies procedure and evade the loss of Fe nanoparticles during the centrifugation and drying process, the phytogenic Fe nanoparticles were added in liquid form. For this, 10 mL of 5 mg/L Cr(VI) solution was treated with freshly prepared 0.2 mL of phytogenic nanoparticles. Effect of different parameters such as nanoparticle dosage (0.1-0.5 mL), initial concentration of Cr(VI) (1-7 mg/L), initial pH of the solution (4-10) and contact time (10-40 min) was also examined. NaOH (1.0 M) and H_2SO_4 1.0 M) were used for the pH adjustment and all the experiments were performed with a duplicate.

Malachite green dye removal studies

MG dye removal experiments were carried out in a 30 mL vial in which the freshly prepared 1mL of phytogenic nanoparticles was treated with 10 mL 50 mg/L dye solution and added 1 mL of H_2O_2 into it. After agitating the solution for 15 minutes using a bath sonicator, the samples were centrifuged to remove the nanoparticles and the residual dye concentration was measured using a UV-visible spectrophotometer. Samples without nanoparticles were also investigated. To study the effect of various parameters, different nanoparticle dosage (1-5 mL), initial concentration of MG dye (10-50 mg/L), pH of the solution (5-9) and contact time (10-40 min) were also investigated.

6.2.3   Characterisation and analytical techniques used

The properties of plant extract were examined by UV-visible spectrophotometer and FTIR. The phytogenic iron nanoparticles were lyophilised using Operon FDU 7003 lyophiliser. The characterisation of prepared nanoparticles was done by HRTEM, EDAX, FTIR and UV-visible spectrophotometer. The details of characterisation techniques were discussed in chapter 2. Fourier transform infrared spectra of the AP and SN plant extracts and AP-Fe and SN-Fe nanoparticles were investigated through Spectrum Two Fourier transform infrared spectrometer (FTIR, Perkin Elmer, USA). Jeol 6390LA/OXFORD XMX N was used to analyse AP-Fe and SN-Fe nanoparticles elemental analysis. GC-MS/MS was used to determine the plant extract components and malachite green degradation products in the solution. The method used in GC-MS/MS analysis has conversed in chapter 3.

6.3. Results and discussion

6.3.1 Characterisation of AP and SN plant extracts

The phytochemical composition of plant extracts has been analysed through GC-MS/MS. Alcohols, phenols, flavonoids, terpenoids, aldehydes, amines and alkanes are the major compounds present in the AP and SN seed coat extracts[8,12]. The mass spectra of identified compounds of AP and SN seed coat extracts by GC-MS/MS are shown in figure 6.2(a1-a8) and figure 6.3(b1-b5) respectively. Biomolecules identified by GC-MS/MS in the AP and SN extracts and their properties were listed in table 6.1. The -OH, -CHO and C=O functional groups in the biomolecules get oxidised into –COOH simultaneously reducing Fe^{3+} ions to Fe nanoparticles. The biomolecules like limonene and 2-hexadecanol act as reducing and stabilising/capping agents, preventing the overgrowth and aggregation of nanoparticles and supporting the reduction of Fe^{3+} ions[13]. Some other biomolecules act as antioxidants that prevent the oxidation of formed nanoparticles and impart more stability.

No.	Retention time (t)	Name of the compound	Molecular weight	Action	Reference
Abrus precautious					
a1.	6.27	furan-2-carbaldehyde	96	Stabilizing agent	[14]
a2.	8.55	1-methyl-4-prop-1-en-2-ylcyclohexene	136	Reducing and capping agent	[15]
a3.	10.21	2,6,6-trimethylbicyclo[3.1.1]hept-2-ene	136	Antioxidant	[16]
a4.	17.25	2,2,4-trimethyl-1H-quinoline	173	Antioxidant	[17]
a5.	23.86	ethyl 3,4,5-trihydroxybenzoate	198	Antioxidant	[18,19]
a6.	12.10	3,5-dihydroxy-6-methyl-2,3-dihydropyran-4-one	144	Antioxidant	[20]
a7.	13.59	5-(hydroxymethyl)furan-2-carbaldehyde	126	Reducing agent	[21]
a8.	20.42	3H-1,3-benzothiazol-2-one	151	Antioxidant	[22]

		Strychnos nux-vomica			
b1.	12.01	1,2-dimethoxybenzene	138	Antioxidant	[23,24]
b2.	12.89	3-methoxy-2-methylpyran-4-one	140	Antioxidant	[25]
b3.	17.23	2,2,4-trimethyl-1H-quinoline	173	Antioxidant	[17]
b4.	18.36	4-methoxy-6-prop-2-enyl-1,3-benzodioxole	192	Antioxidant	[26]
b5.	21.73	hexadecan-2-ol	242	Reducing and stabilising agent	[27]

Table 6.1 *Biomolecules identified in AP and SN extract by GC-MS/MS*
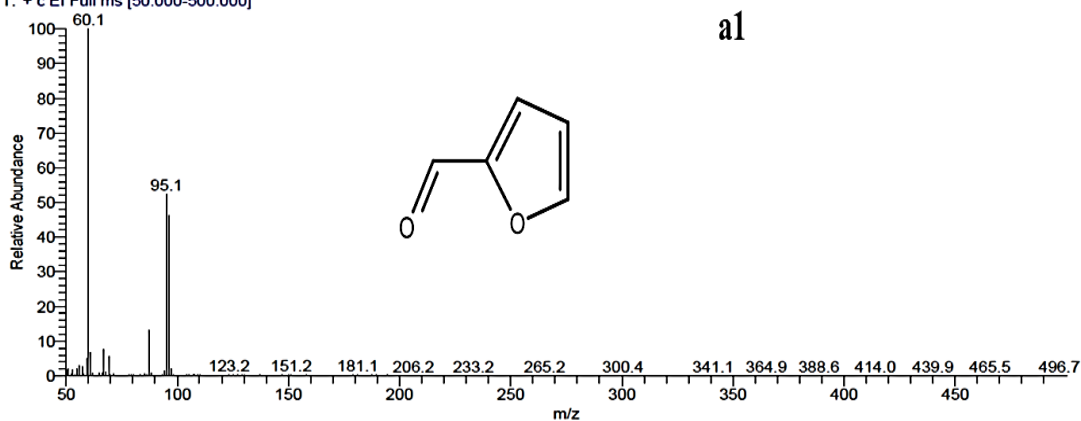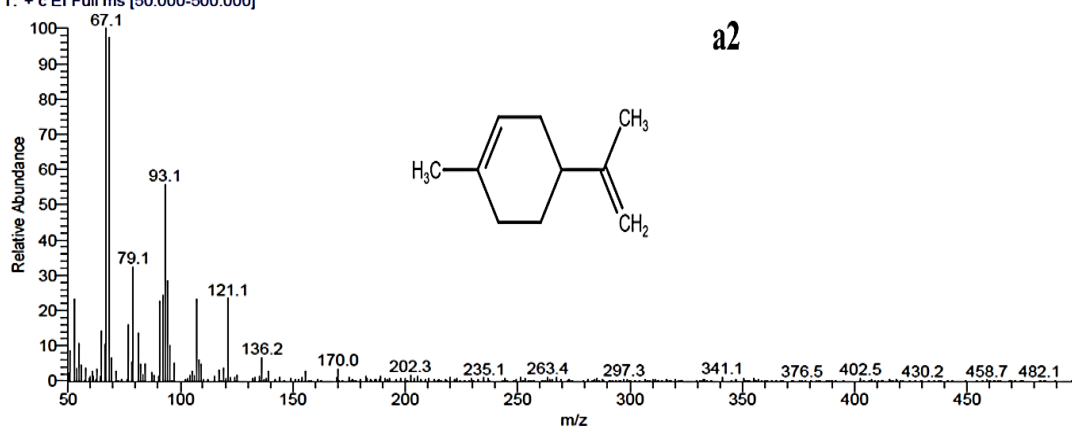
AP #1828   RT: 10.21   AV: 1   AV: 5   SB: 12 1821-1826 1830-1835   NL: 1.24E6
T: + c EI Full ms [50.000-500.000]

a3
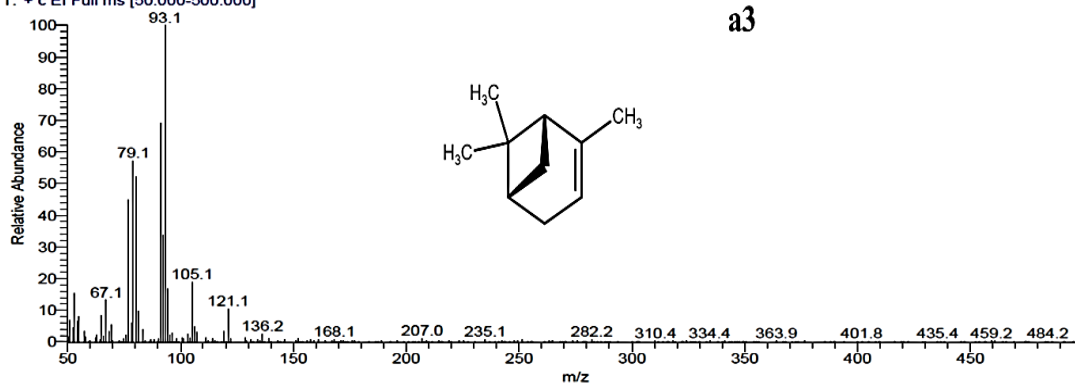
AP #3897   RT: 17.25   AV: 1   AV: 5   SB: 12 3890-3895 3899-3904   NL: 1.62E7
T: + c EI Full ms [50.000-500.000]

a4
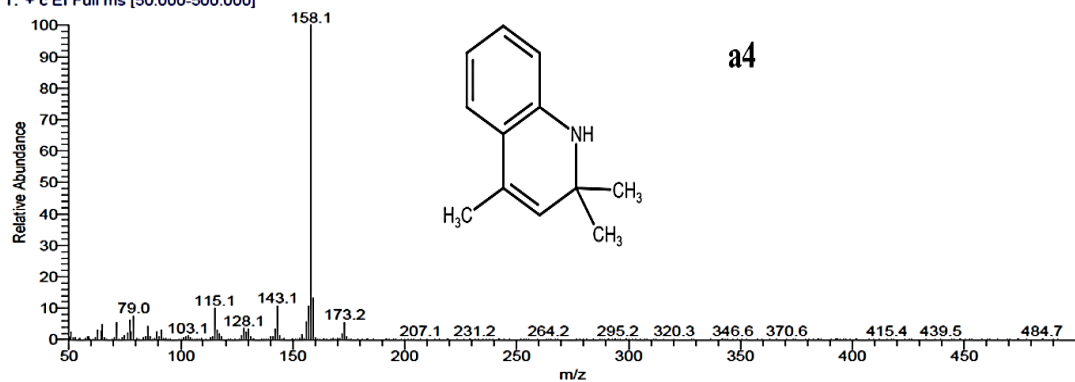
AP #5839   RT: 23.86   AV: 1   AV: 5   SB: 12 5832-5837 5841-5846   NL: 6.88E6
T: + c EI Full ms [50.000-500.000]

a5
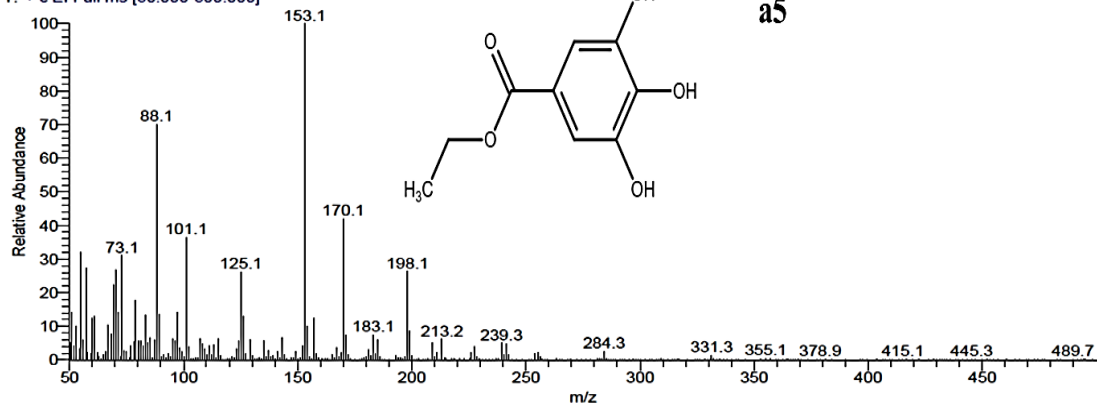
AP #2383   RT: 12.10   AV: 1   AV: 5   SB: 12 2376-2381 2385-2390   NL: 5.43E5
T: + c EI Full ms [50.000-500.000]

a6
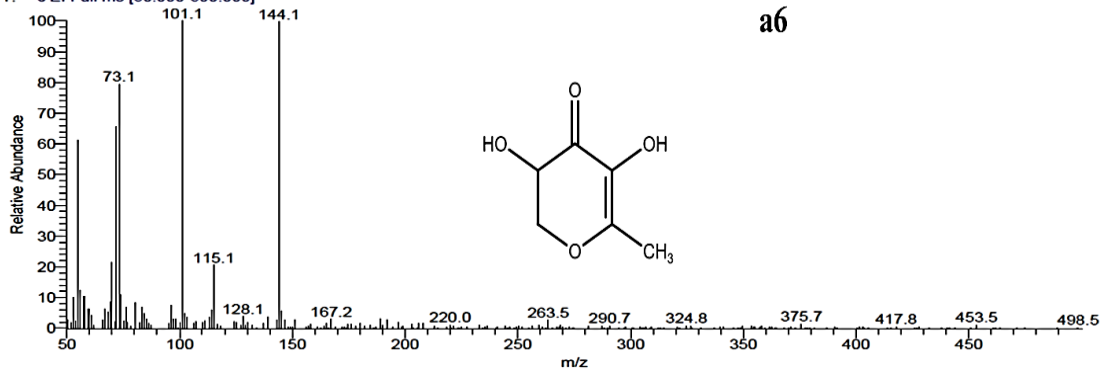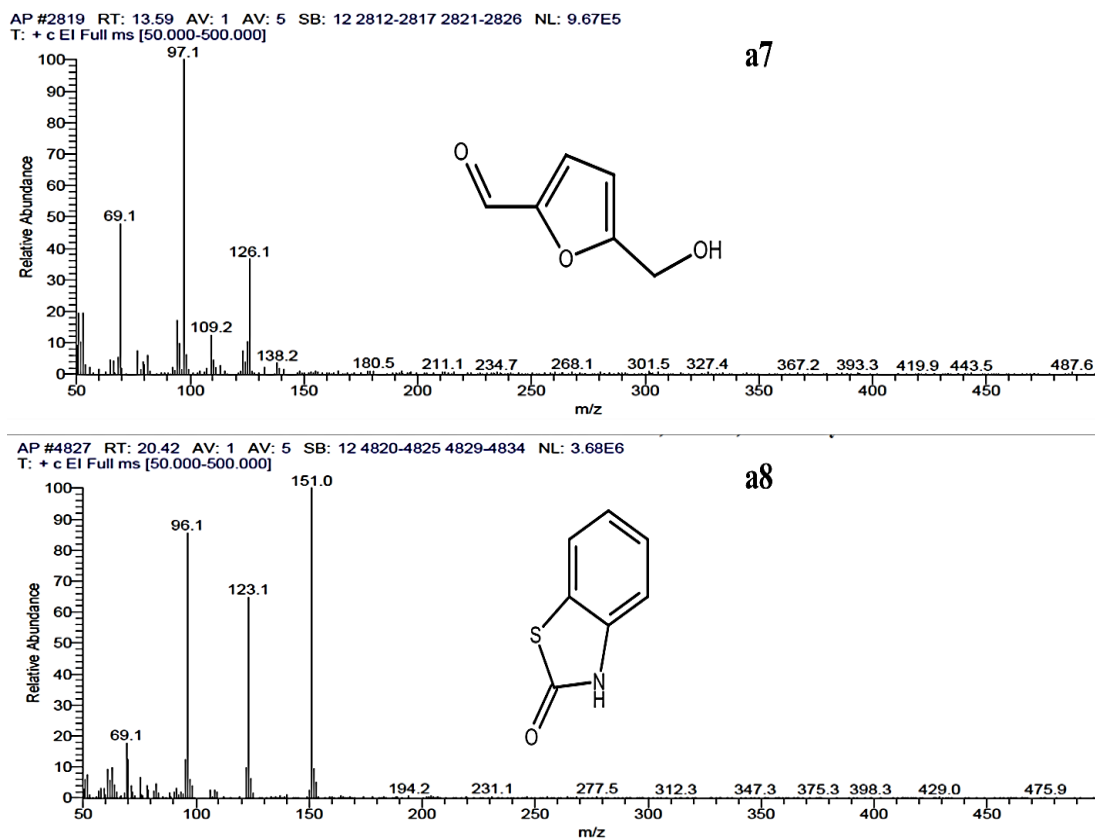
Figure 6.2 *Mass spectra of compounds identified in AP extract by GC-MS/MS. (a1) furan-2-carbaldehyde; (a2) 1-methyl-4-prop-1-en-2-ylcyclohexene; (a3) 2,6,6-trimethylbicyclo [3.1.1]hept-2-ene; (a4) 2,2,4-trimethyl-1H-quinoline; (a5) ethyl 3,4,5-trihydroxybenzoate ; (a6) 3,5-dihydroxy-6-methyl-2,3-dihydropyran-4-one; (a7) 5-(hydroxymethyl)furan-2-carbaldehyde; (a8) 3H-1,3-benzothiazol-2-one*
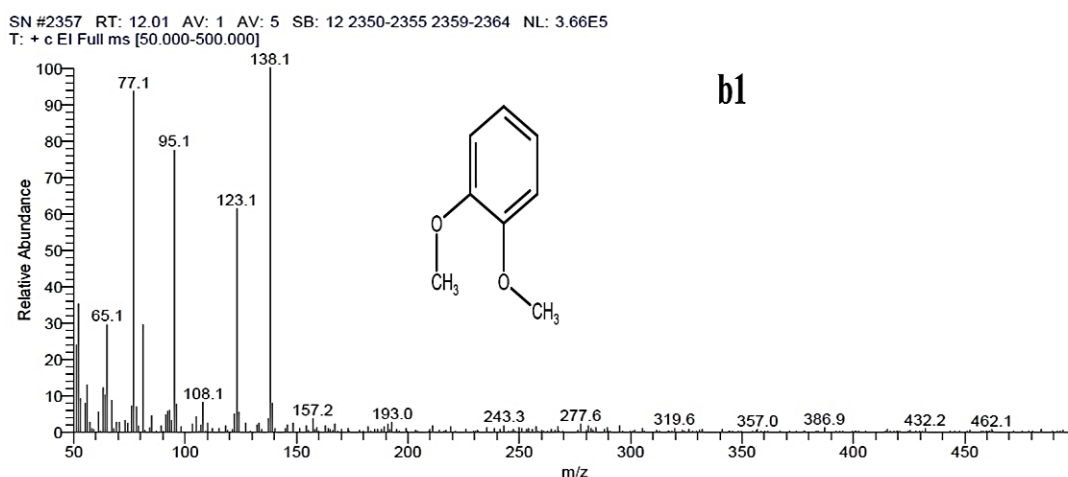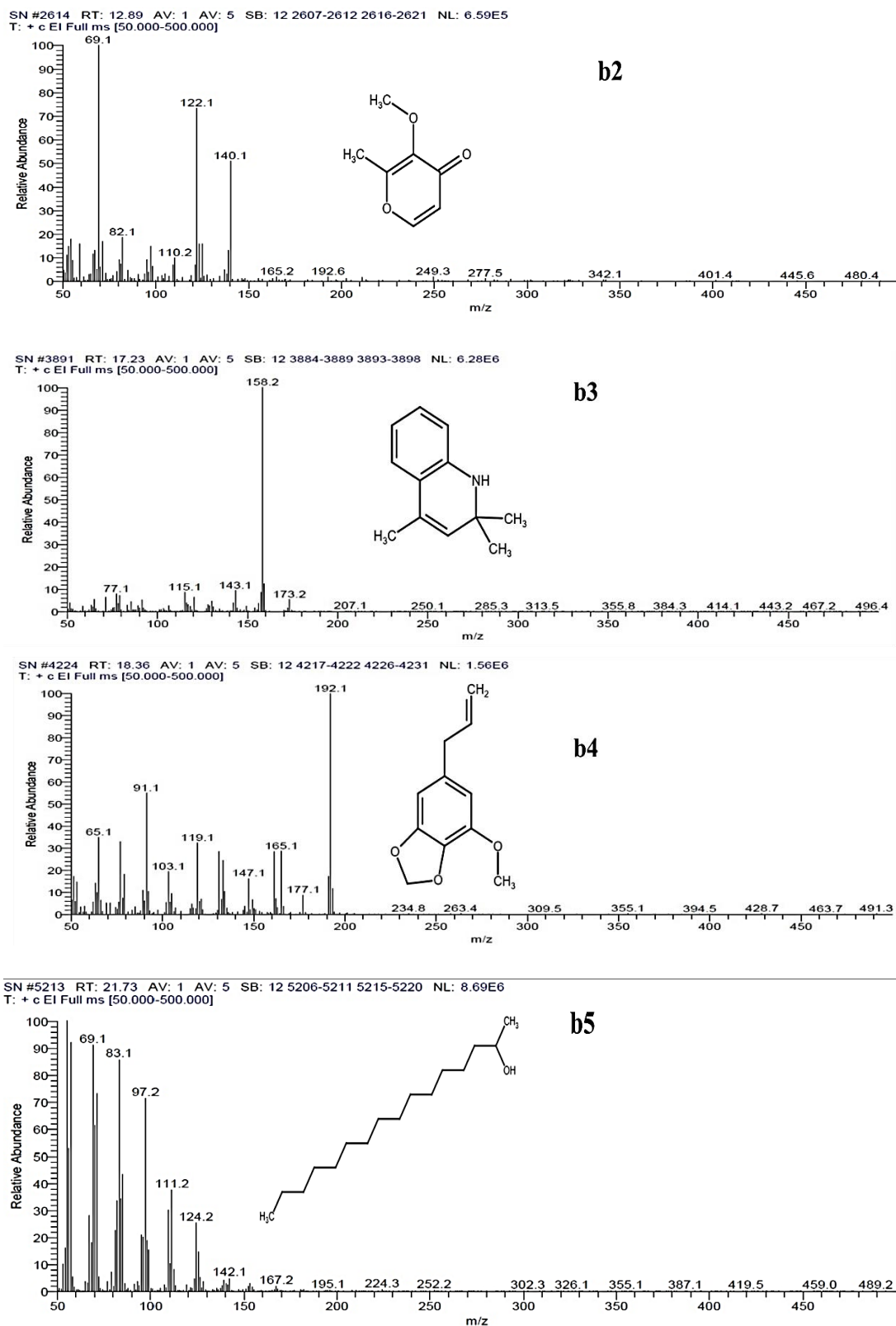
Figure 6.3 Mass spectra of compounds identified in SN extract by GC-MS/MS. (b1) 1,2-dimethoxybenzene; (b2) 3-methoxy-2-methylpyran-4-one; (b3) 2,2,4-trimethyl-1H-quinoline; (b4) 4-methoxy-6-prop-2-enyl-1,3-benzodioxole; (b5) hexadecan-2-ol

6.3.2 Characterisation of AP-Fe and SN-Fe nanoparticles

UV-visible spectroscopy

A dark black solution was formed immediately when the plant extracts were mixed with FeCl₃ solution, indicating the formation of Fe nanoparticles[28]. The black precipitates in the solution were visually observable; however, the formation of iron nanoparticles was further confirmed by a UV-visible spectrophotometer. The UV-visible spectra of AP and SN extract, FeCl₃ solution and phytogenic iron nanoparticles are shown in figure 6.4. The FeCl₃ solution and plant extracts did not show any characteristic peak in UV-visible spectra between 450-750 nm. Nevertheless, the AP-Fe and SN-Fe nanoparticles showed broad adsorption around this region, indicating the formation of Fe nanoparticles[29].
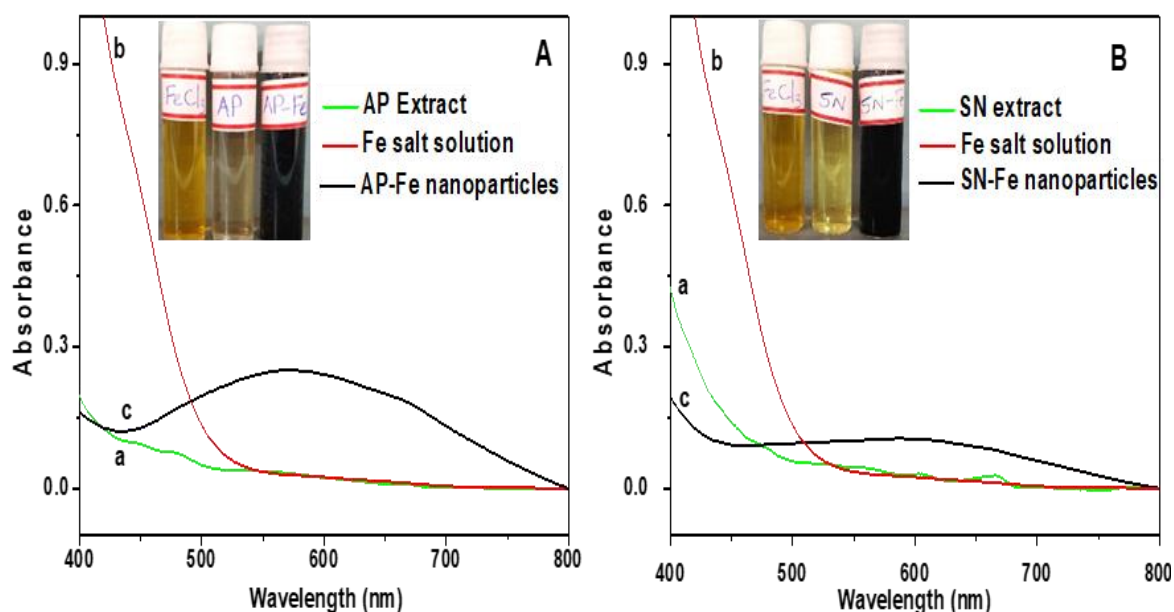
Figure 6.4 *Photographs and UV-visible spectra of A) a. AP extract, b. FeCl₃ solution and c. AP-Fe nanoparticles, B) a. SN extract, b. FeCl₃ solution and c. SN-Fe nanoparticles*

HRTEM

HRTEM photographs of AP-Fe and SN-Fe nanoparticles are shown in figure 6.5. The spherical SN-Fe nanoparticles are non-agglomerated and monodispersed. It can be due to the stabilisation by the major components of SN, such as strychnine and brucine. The particle size of SN-Fe nanoparticles ranged from 2.1 to 5 nm, having a mean diameter of 3.3 nm. SAED analysis of SN-Fe nanoparticles shows faded spots and diffused rings, which indicate the nanoparticles amorphous nature. The d-spacing values 2.73 Å and 2.14 Å calculated from the SAED pattern match with the (220) and (311) planes of the

Fe_3O_4[30]. AP-Fe nanoparticles were irregularly shaped with size ranging from 3 nm to 32 nm. SAED pattern comprised of spot patterns with diffused rings indicates the presence of dispersed crystalline particles over the amorphous phase of AP-Fe. AP extract contains plant components with different reducing and complexing capacities, leading to the formation of different Fe nanoparticles such as Fe^0 and Fe_3O_4. SAED pattern displays d-spacing values 2.0 Å and 2.89 Å corresponding to (311) and (213) plane of Fe^0[31]. The d- spacing values of 2.7 Å corresponds to the planes of Fe_3O_4[32].
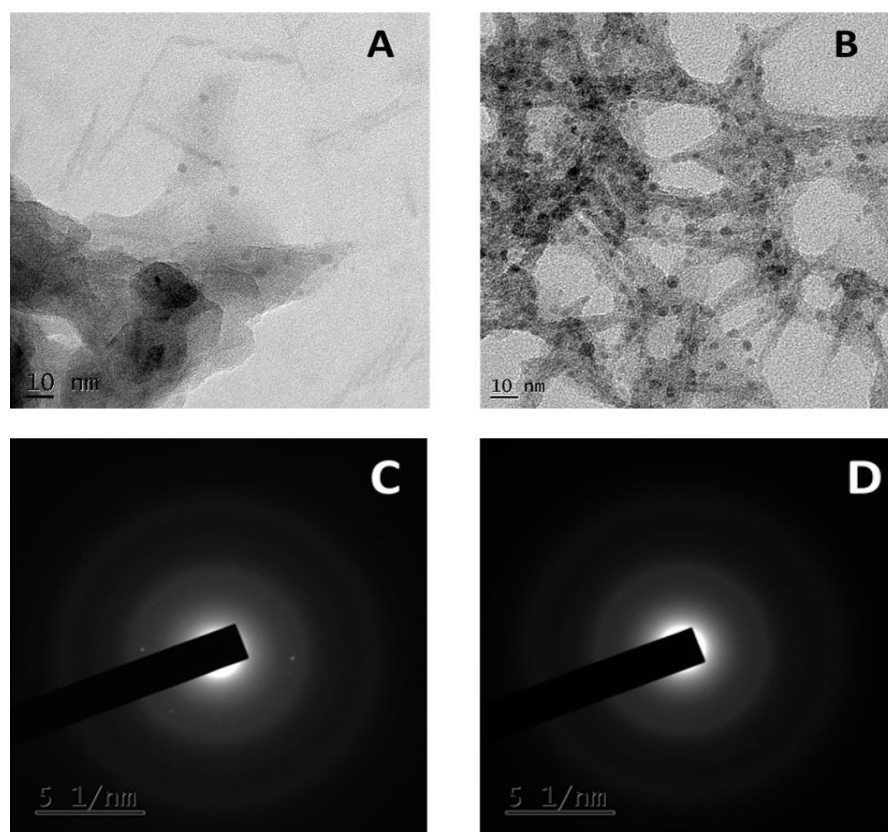
***Figure 6.5** TEM image of the synthesised A) AP-Fe nanoparticles and B) SN-Fe nanoparticles and SAED pattern of C) AP-Fe nanoparticles and D) SN-Fe nanoparticles*

EDAX

The qualitative and quantitative information of nanoparticles and the elements involved in the formation of nanoparticles has been studied through EDAX analysis. As shown in figure 6.6, the AP-Fe and SN-Fe nanoparticles depict intense peaks of Fe, C and O. The results reveal that the atomic percentages of iron in AP-Fe and SN-Fe nanoparticles were 7.57 and 7.15 respectively. The presence of C, O, Ca and K may be from the organic

coating on the iron nanoparticles and the presence of chlorine from the ferric chloride which is used as the iron precursor during the synthesis of nanoparticles.
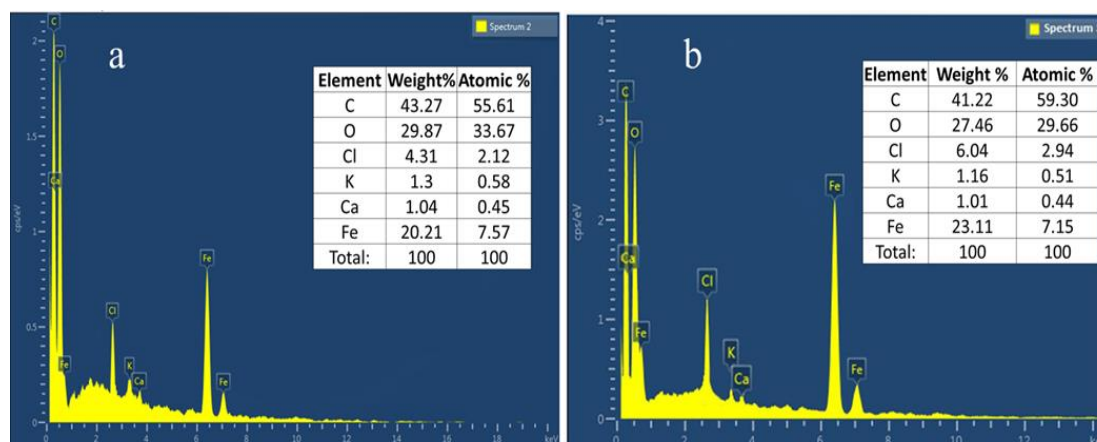
Figure 6.6 *EDAX spectra of a) AP-Fe nanoparticles and b) SN-Fe nanoparticles*

FTIR spectroscopy

The FTIR spectra of the AP-Fe and SN-Fe nanoparticles are shown in figure 6.7. It envisages the functional groups in bioactive components responsible for the formation and stabilisation of iron nanoparticles. The phytogenic nanoparticles showed a broad peak between 3700-3000 cm^{-1}, corresponding to O-H stretching and N-H stretching bands of polyphenols and amines respectively[33]. The peaks at 1725 cm^{-1} (AP-Fe) and 1719 cm^{-1} (SN-Fe) corresponds to the C=O stretching vibrations and the peaks at 1425 cm^{-1} (AP-Fe) and 1416 cm^{-1} (SN-Fe) corresponds to the O-H bending vibrations of -COOH group present in the phytogenic Fe nanoparticles. The peaks found at 1195 cm^{-1} for AP-Fe and 1192 cm^{-1} and 1035 cm^{-1} for SN-Fe is related to the C-N stretching vibrations and the peaks at 1579 cm^{-1} (AP-Fe) and 1581 cm^{-1} (SN-Fe) corresponds to the N-H bending vibrations of amines present in the plant component. The presence of aromatic amine was confirmed through C-N stretching vibrations which shows the peak at 1334 cm^{-1} for AP-Fe and 1328 cm^{-1} for SN-Fe nanoparticles. The peaks that appeared at 2925 cm^{-1} and 2856 cm^{-1} for AP-Fe and 2921 cm^{-1} and 2850 cm^{-1} for SN-Fe were associated with the C-H stretching vibrations. The stretching vibrations of C=C peaks at 1615 cm^{-1} and 1620 cm^{-1} correspond to AP-Fe and SN-Fe nanoparticles. The peaks observed at 1069 cm^{-1} (AP-Fe) and 1072 cm^{-1} (SN-Fe) indicates the O-H stretching vibrations of alcohol. The low intense peaks at 671 cm^{-1} (AP-Fe) and 679 cm^{-1} (SN-Fe) corresponds to the iron-carbonyl complexes (Fe–C=O), which confirmed the iron interaction with the plant components[34]. The peaks at 446 cm^{-1} and 467 cm^{-1} confirm the Fe-O stretching vibration

of iron oxide present in the AP-Fe and SN-Fe nanoparticles[35]. The results envisage that plant components cling on the surface of Fe nanoparticles as capping agents and are part of the Fe nanoparticles. This organic moiety increases the stability of the Fe nanoparticles.
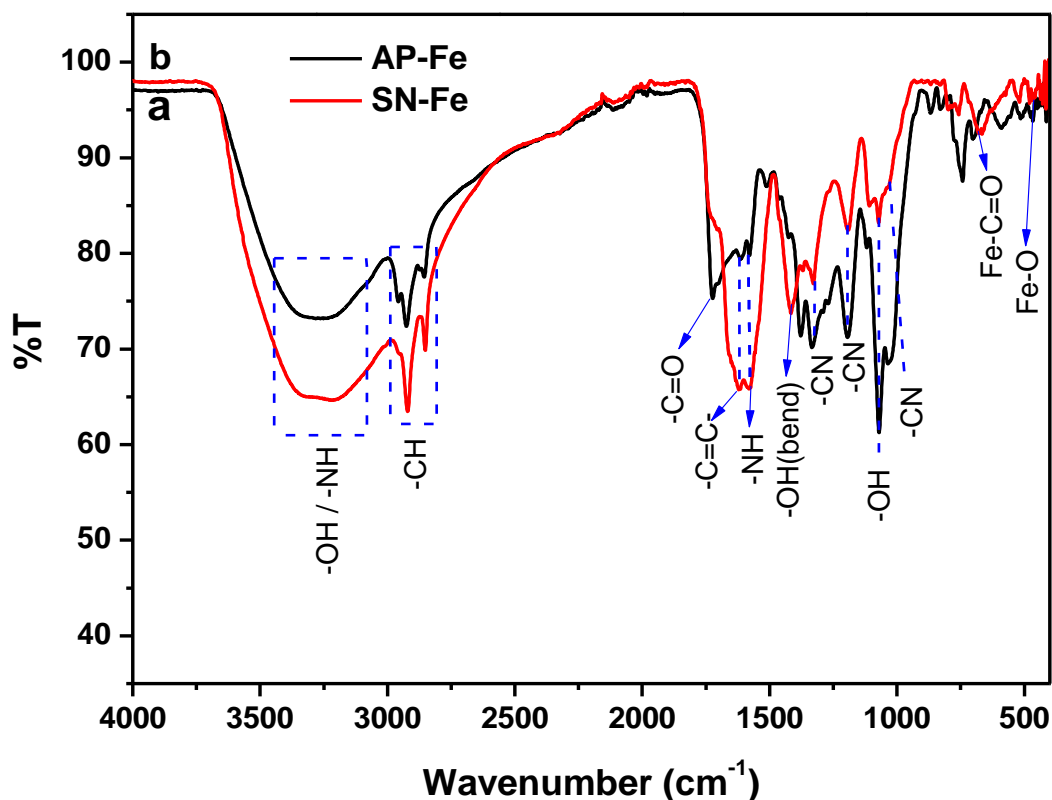
Figure 6.7 FTIR spectra of a) AP-Fe nanoparticles and b) SN-Fe nanoparticles

6.3.3 Cr(VI) removal studies

The Cr(VI) removal efficiency of AP-Fe and SN-Fe nanoparticles was evaluated using 0.2 mL phytogenic nanoparticles in 10 mL, 5 mg/L Cr(VI) solution for 15 minutes, as shown in figure 6.8. The AP-Fe and SN-Fe nanoparticles showed 73 % and 69 % removal efficiency which indicate that AP-Fe nanoparticles exhibit more Cr(VI) removal efficiency than SN-Fe nanoparticles. This is attributed to the composition of AP-Fe nanoparticles since they contain zero valent iron and iron oxide nanoparticles. Zero valent iron nanoparticles have shown more Cr(VI) reduction capacity than iron oxide nanoparticles[36]. The removal of Cr(VI) using phytogenic Fe nanoparticles displays reduction, precipitation and adsorption of chromium species[37,38]. The possible Cr(VI) removal mechanism of AP-Fe and SN-Fe nanoparticles was proposed in equations 6.1-6.6.

1. Adsorption process

$$Cr(VI) + AP - Fe \rightarrow Cr(VI)/AP - Fe \tag{6.1}$$

$$Cr(VI) + (AP/SN) - Fe_2O_3 \rightarrow Cr(VI)/(AP/SN) - Fe_3O_4 \tag{6.2}$$

$$Fe^{2+}/Fe^{3+} + H_2O \rightarrow FeOOH \tag{6.3}$$

$$Cr(VI) + FeOOH \rightarrow Cr(VI) - FeOOH \tag{6.4}$$
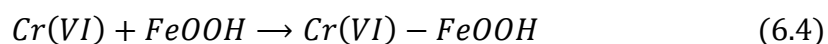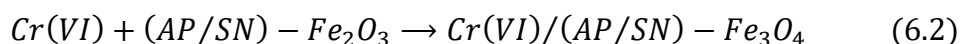
2. Reduction and precipitation process

$$2Fe^0 + Cr_2O_7^{2-} + 8H^+ \rightarrow 3Fe^{2+} + 2Cr(OH)_3 + H_2O \tag{6.5}$$

$$6Fe^{2+} + Cr_2O_7^{2-} + 8H^+ \rightarrow 6Fe^{3+} + 2Cr(OH)_3 + H_2O \tag{6.6}$$
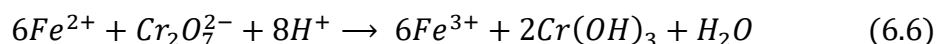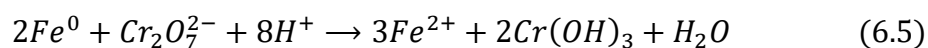
In addition to this, plant components present in the solution also have an important role in removing Cr(VI). Plant extracts have different bioactive components which help to form Fe nanoparticles by acting as reducing and stabilising agents. These plant components may also have the capacity to remove Cr(VI) from water[36]. Overall, the phytogenic Fe nanoparticles display good Cr(VI) removal efficiency.

As per previous reports, different parameters influence Cr(VI) removal using phytogenic Fe nanoparticles. The influence of these parameters such as nanoparticle dosage, initial concentration of Cr(VI), initial pH of the Cr(VI) solution and contact time were investigated for Cr(VI) removal.
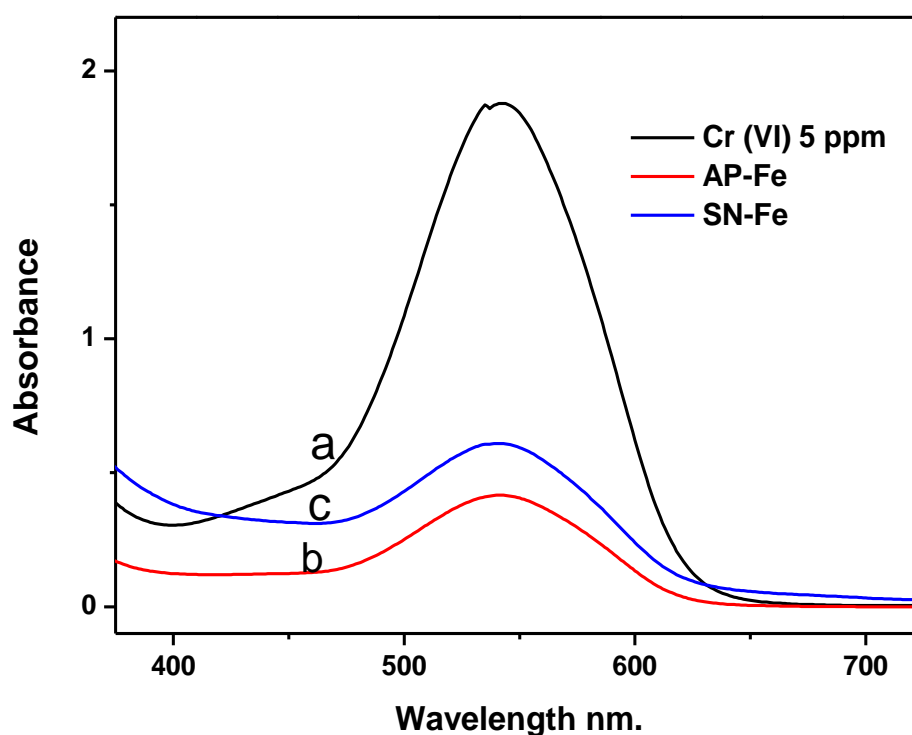
Figure 6.8 *UV-visible spectra of Cr(VI) solution after treating 15 minutes a) blank Cr(VI) 5 mg/L, b) AP-Fe nanoparticles and c) SN-Fe nanoparticles*

Effect of nanoparticle dosage

The effect of nanoparticle dosage was studied by varying the nanoparticles dosage from 0.1 mL to 0.5 mL, maintaining 5 mg/L as the initial concentration of Cr(VI) and 15 minutes as the contact time. Figure 6.9a indicates that the increased nanoparticle dosage enhances the extent of Cr(VI) removal. AP-Fe nanoparticles exhibit 100 % Cr(VI) removal using a dosage of 0.4 mL, while using the same quantity, SN-Fe nanoparticles exhibit only 76 % removal. The maximum removal attained by SN-Fe nanoparticles was 80 % using 0.5 mL nanoparticles. With the increase in nanoparticle dosage, the reactive sites for reduction and adsorption were also increased, leading to the higher removal of Cr(VI) ions. In short, AP-Fe nanoparticles show more potential to reduce Cr(VI) than SN-Fe nanoparticles.

Effect of the initial concentration of the Cr(VI) solution

As shown in figure 6.9b, the effect of initial Cr(VI) concentration on Cr(VI) removal was investigated while keeping all other parameters constant. In this study, 0.2 mL nanoparticle solution was added into different Cr(VI) concentrations, varied from 1 mg/L to 7 mg/L and the absorbance was measured after 15 minutes. When the chromium concentration was 1 mg/L, 100 % Cr(VI) removal occurred in AP-Fe nanoparticles and 89 % Cr(VI) removal occurred in SN-Fe nanoparticles. However, in 7 mg/L Cr(VI) solution, the removal percentage decreases to 71 % by AP-Fe nanoparticles and 58 % by SN-Fe nanoparticles. So with the increase in Cr(VI) concentration, naturally there occurs a decrease in the availability of sufficient reactive sites, for Cr(VI) ions, which eventually leads to the decrease in Cr(VI) removal efficiency.

Effect of contact time

The effect of contact time was studied by adding 0.2 mL phytogenic nanoparticles into 5 mg/L Cr(VI) solution and the samples were collected at regular time intervals of 10, 20, 30 and 40 minutes. As shown in figure 6.9c, Cr(VI) removal efficiency increases with increasing contact time, even though the increase in rate is not high. 67 % and 60 % of removal were observed for the first 10 minutes of contact time by AP-Fe and SN-Fe nanoparticles respectively. However, for 40 minutes of contact time, the Cr(VI) removal efficiency was 80 % and 71 % for AP-Fe and SN-Fe nanoparticles. This may be due to the fact that with the increase in contact time, the Cr(VI) molecules have more time to interact with the AP-Fe and SN-Fe nanoparticles and the removal efficiency increases. As time

proceeds, iron gets exceedingly oxidised and the adsorption sites become blocked by precipitation leading to decreased Cr(VI) removal rate.
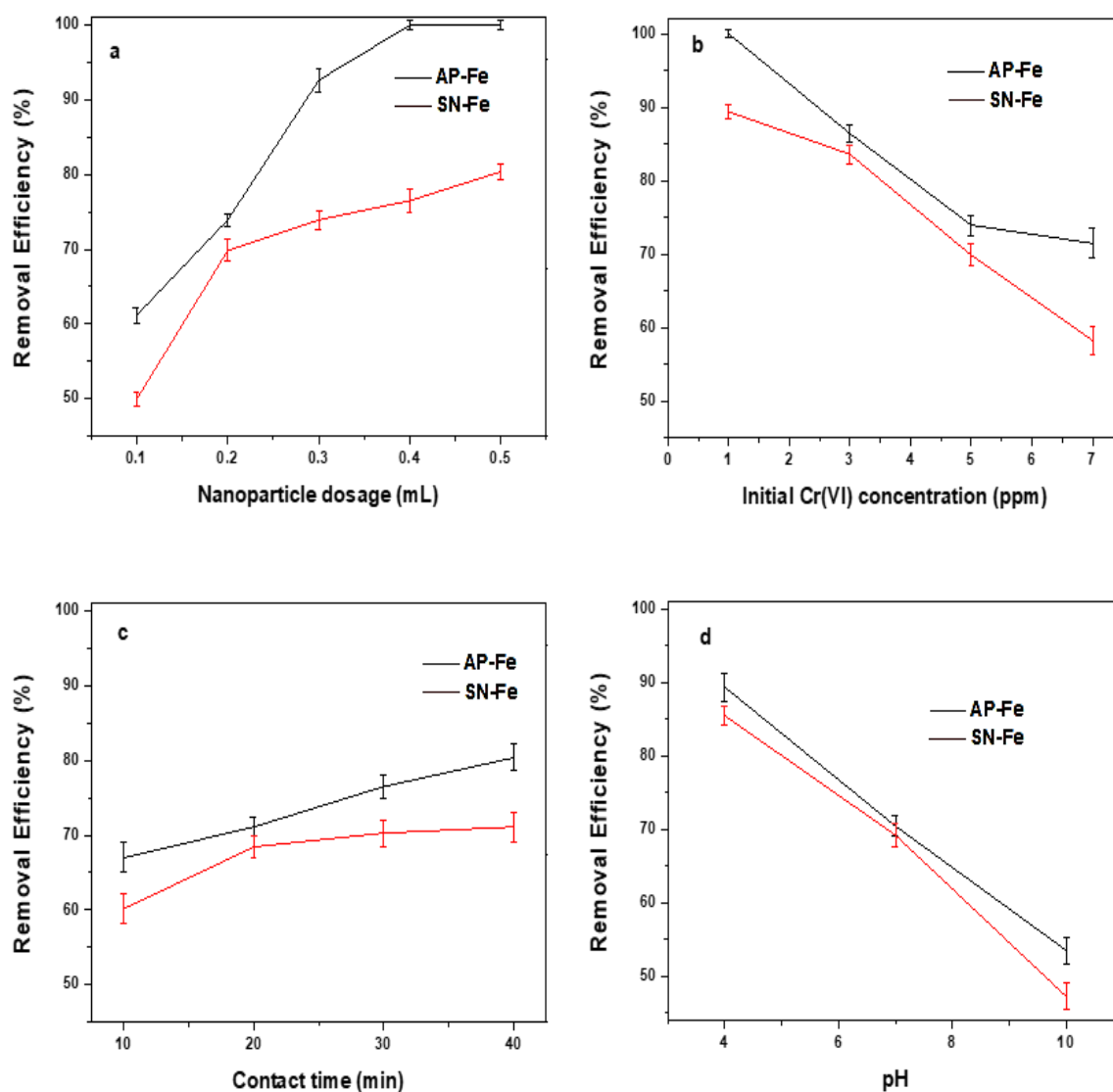
Figure 6.9 *Effects of various factors on Cr(VI) removal: (a) nanoparticle dosage, (b) initial Cr(VI) concentration, (c) contact time and (d) initial solution pH .*

Effect of pH

The initial pH of the solution greatly influences the efficiency of Cr(VI) removal. With 0.2 mL nanoparticles in 5 mg/L Cr(VI) solution, the effect of initial pH was evaluated at three pH values viz 4, 7 and 10. As shown in figure 6.9d, the Cr(VI) removal efficiency decreases with the increase of the initial solution pH. At pH 4, the AP-Fe and SN-Fe nanoparticles remove 89 % and 85 % of Cr(VI) respectively, which gradually reduces to 53 % and 47 % at pH 10. The initial pH of the solution influences the surface charge and

distribution of reactive sites in the phytogenic Fe nanoparticles and the speciation of Cr(VI) ions in the aqueous solution[39]. At lower pH, the dominant form of Cr(VI) was $HCrO_4^-$, the hydrolysis product of $Cr_2O_7^{2-}$[29]. This Cr(VI) form get reduced in the presence of H^+ ions in acidic solution as follows

$$2HCrO_4^- + 3Fe^0 + 14H^+ \longrightarrow 3Fe^{2+} + 2Cr^{3+} + 8H_2O \qquad (6.7)$$

$$2HCrO_4^- + 6Fe^{2+} + 14H^+ \longrightarrow 6Fe^{3+} + 2Cr^{3+} + 8H_2O \qquad (6.8)$$
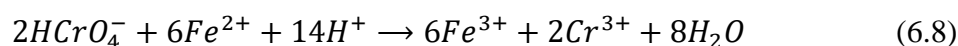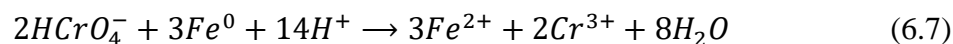
In addition to this, the electrostatic attraction between negatively charged $HCrO_4^-$ and positively charged Fe nanoparticles surface is intense in acidic conditions, which leads to the more adsorption of Cr(VI) species[29,39].

At pH value > 6, the dominant Cr(VI) species was $Cr_2O_4^{2-}$ which compete with the OH^- ions for adsorptive sites of phytogenic Fe nanoparticles, leading to decreased removal efficiency. Furthermore, in basic pH, the formation of the oxide passive layer in the Fe nanoparticles hinders the Fe nanoparticle's extent of corrosion and leads to the decline of Cr(VI) removal efficiency[39,40].

6.3.4 MG dye removal studies

Fenton's reaction is extensively studied to degrade toxic dyes due to its high efficiency and low cost. In this catalytic process, an iron catalyst produces hydroxyl radicals (·OH) from hydrogen peroxide (H_2O_2). The formed ·OH radicals interact with the dye molecules and form new oxidised low molecular weight intermediates which are finally converted to CO_2 and H_2O by the continued action of ·OH radicals[41]. MG dye removal studies were conducted in the presence of H_2O_2 to evaluate the reactivity of the synthesised Fe nanoparticles. In dye removal, the influence of initial dye concentration, pH, contact time and nanoparticle dosage were also examined. Generally, MG exhibits three absorbance peaks in the UV-visible spectrum. The characteristic peak is seen at 617 nm (-C-N- bond) and absorbance due to associated aromatic rings are seen at 424 and 316 nm[42]. As shown in figure 6.10, the best results occurred when the phytogenic Fe nanoparticles were used, while negligible MG removal was observed using H_2O_2 only. AP-Fe nanoparticles removed approximately 98 % of MG within 15 minutes, higher than SN-Fe (91 %) nanoparticles. While reacting with phytogenic Fe nanoparticles, the intensity of the MG characteristic peak decreased, two minor peaks disappeared and a new peak formed around

360 nm. It may be due to the cleavage of the -C=C- bond and destruction of MG conjugated structures[43]. The high intensity below 275 nm could be due to the polyphenols present in the phytogenic Fe nanoparticles and the degraded products of MG[44]. The possible mechanism of MG dye removal using phytogenic Fe nanoparticles are 1) Adsorption of MG and its degraded products into Fe/Fe_3O_4 capped with plant component and 2) degradation of MG molecule due to the ·OH radicals produced through reaction with H_2O_2[42]. The high activity of AP-Fe nanoparticles was owing to the formation of more ·OH radicals compared to SN-Fe nanoparticles since Fe^0 have more zero valent iron. The MG removal process can be explained as equation 6.9-6.17.
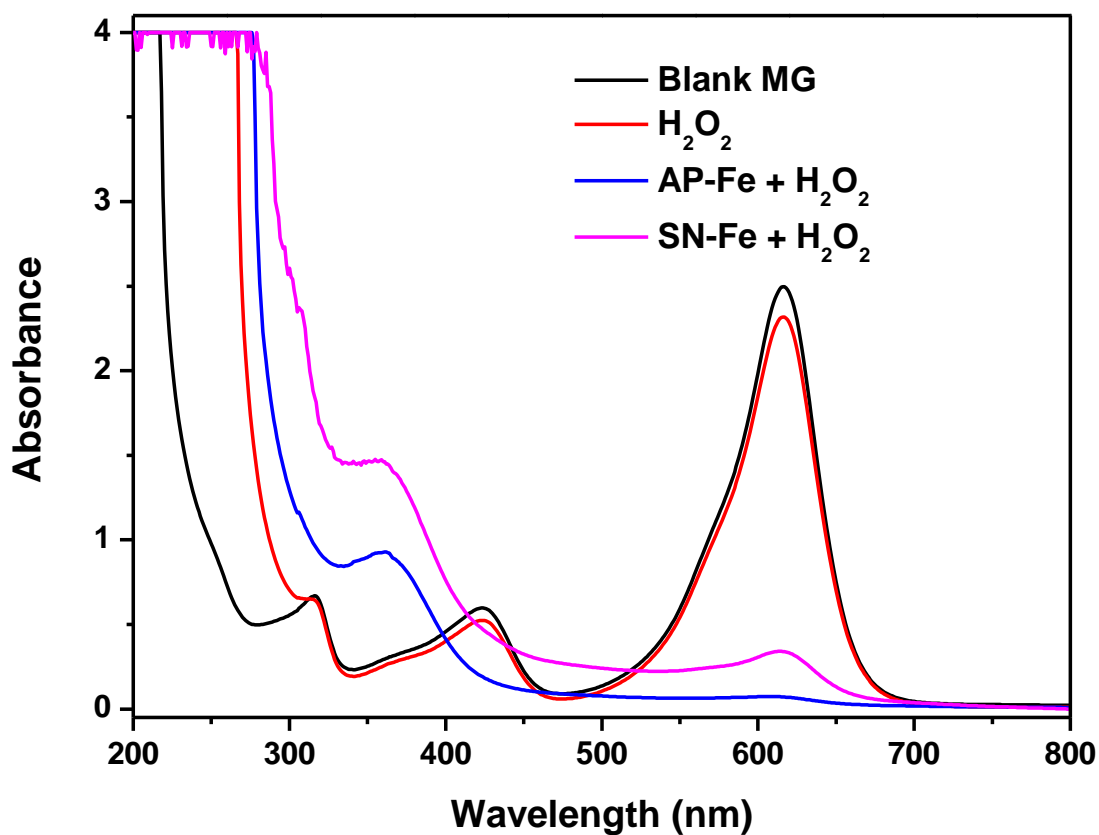
Figure 6.10 *UV-visible spectra of MG dye solution after treating 15 minutes*
a) blank MG 50 mg/L, b) AP-Fe nanoparticles and c) SN-Fe nanoparticles

1. Adsorption process:

$$MG + AP - Fe \rightarrow MG/AP - Fe \qquad (6.9)$$

$$MG + (AP/SN) - Fe_3O_4 \rightarrow MG/(AP/SN) - Fe_3O_4 \qquad (6.10)$$
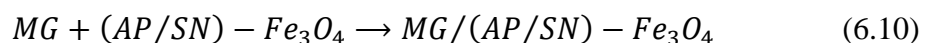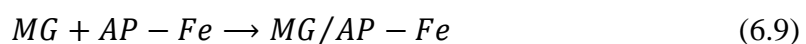
2. Degradation of MG dye through the attack of the ·OH radicals:

$$Fe^0 + H_2O_2 \longrightarrow Fe^{2+} + 2OH^- \tag{6.11}$$

$$Fe^{2+} + H_2O_2 \longrightarrow Fe^{3+} + OH^- + \cdot OH \tag{6.12}$$

$$Fe^{3+} + H_2O_2 \longrightarrow Fe^{2+} + H^+ + HO_2\cdot \tag{6.13}$$

$$Fe^{2+}/Fe^{3+} + H_2O \longrightarrow FeOOH \tag{6.14}$$

$$MG + Fe_3O_4/FeOOH \longrightarrow MG - (Fe_3O_4 \,/\, FeOOH) \tag{6.15}$$

$$MG - (Fe_3O_4/FeOOH) + \cdot OH \longrightarrow MG\ degradation\ products \tag{6.16}$$

$$MG\ degradation\ products + \cdot OH \longrightarrow CO_2 + H_2O \tag{6.17}$$
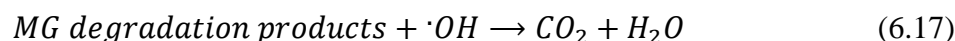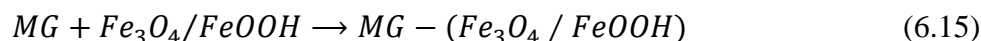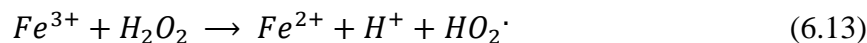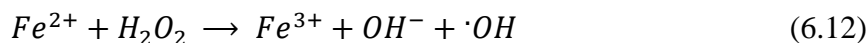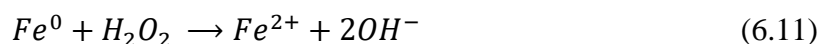
Effect of nanoparticle dosage

Dosage of phytogenic Fe nanoparticles significantly influences the MG dye removal. As shown in figure 6.11a, the MG dye removal efficiency increased from 98 % to 100 % in AP-Fe nanoparticles and 91 % to 96 % in SN-Fe nanoparticles as the nanoparticle dosage increased from 1 to 2.5 mL. The MG dye concentration and contact time were kept constant at 50 mg/L and 15 min. MG removal is attributed to increased Fe^{2+} availability for the hydroxyl radical formation with nanoparticle dosage. With the increase in hydroxyl radicals formation, more dye molecules get degraded. In addition, total adsorption sites were increased with an increase in phytogenic Fe nanoparticles, which eventually led to the adsorption of more dye molecules and their degraded products.

Effect of the initial concentration of the MG

The effect of the initial concentration of MG on the removal of MG dye is shown in figure 6.11b. The dosage of nanoparticles and contact time were kept constant as 1 mL and 15 minutes respectively. The AP-Fe nanoparticles show 98 to 100 % removal and SN-Fe nanoparticles shows 91 % to 97 % removal when the MG concentration decreases from 50 mg/L to 10 mg/L. The efficiency for the removal of MG decreased with the increasing initial concentration of MG. The decrease in MG removal efficiency with increased concentration is attributed to the insufficiency of hydroxyl radicals and adsorption sites required for dye degradation.

Effect of contact time

Contact time is another crucial parameter influencing the removal efficiency of MG dye. The effect on the removal of MG having 50 mg/L concentration was studied at different time intervals using 1 mL of AP-Fe nanoparticles and SN-Fe nanoparticles, as shown in

figure 6.11c. The percentage of removal efficiency increases with an increase in contact time from 10 minutes to 40 minutes. AP-Fe nanoparticles attained 100 % removal efficiency within 30 minutes. At the same time, SN-Fe nanoparticles only attained 94 % removal efficiency. The interaction between hydroxyl radical and dye molecule increases with increasing contact time leading to more dye removal.

Effect of pH

The degradation of MG by AP-Fe nanoparticles and SN-Fe nanoparticles were studied at initial pH values of 5, 7 and 9 as shown in figure 6.11d. The removal efficiency of the AP-Fe nanoparticles and SN-Fe nanoparticles was decreased with an increase in pH value. At pH 5, the AP-Fe nanoparticles attained 100 % and SN-Fe nanoparticles exhibited 96 % removal efficiency. As the pH increases, iron hydroxide precipitation decreases the MG removal efficiency.
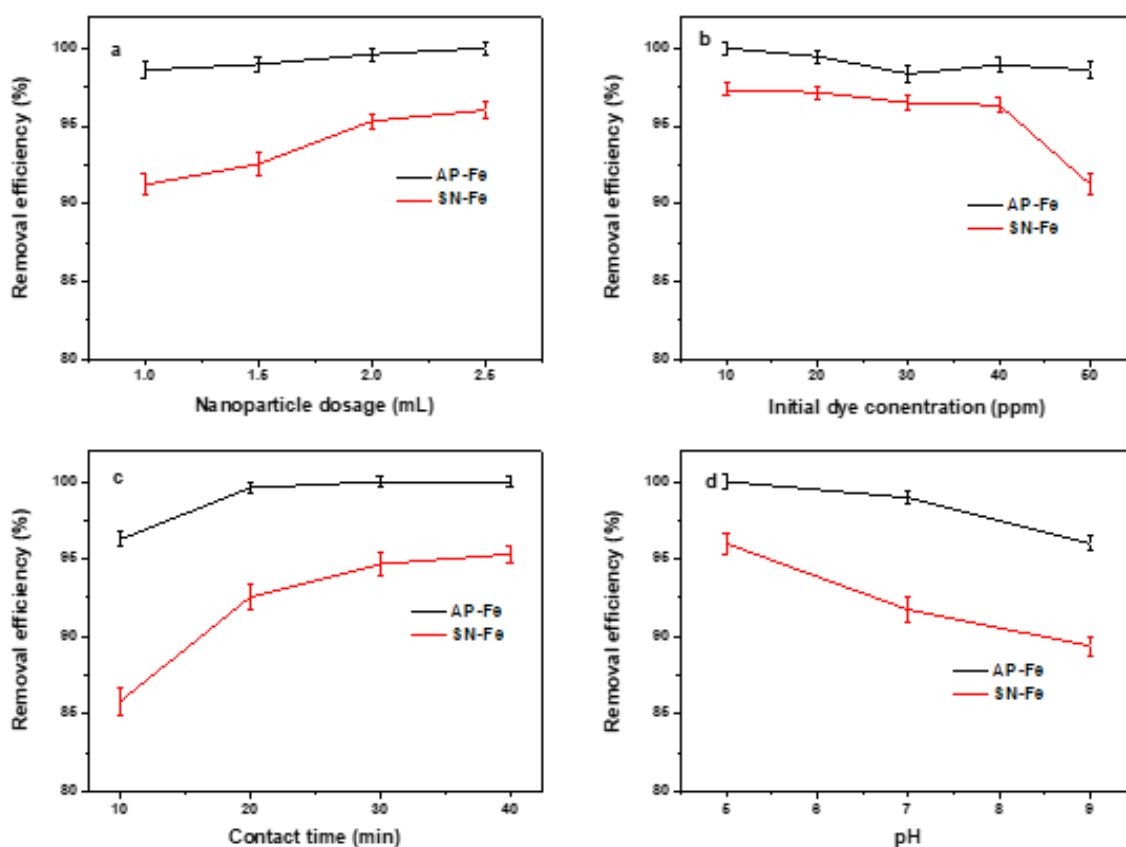
Figure 6.11 *Effects of various factors on MG removal (a) nanoparticle dosage, (b) initial MG concentration, (c) contact time and (d) initial solution pH.*

GC-MS/MS analysis

The GC-MS/MS analysis of malachite green after treating with AP-Fe nanoparticles confirmed the degradation of MG dye molecules. The GC-MS/MS analysis shows the presence of [4-(dimethylamino)phenyl]-phenylmethanone (Rt 21.28, MW 225), benzoic acid (Rt 12.23, MW 122) and diphenylmethanone (Rt 19.91, MW 182) in the solution. Among the three degradation products, benzoic acid is not detected in our previous studies. The MS spectra and structure of benzoic acid are shown in figure 6.12. Hydroxyl radical attack on the [3-hydroxy-4-(methylamino)phenyl]-phenylmethanone causes the formation of benzoic acid[45] as shown in scheme 6.1. The creation of [3-hydroxy-4-(methylamino)phenyl]-phenylmethanone, a degradation product of malachite green dye is discussed in chapter 3. The results show that the addition of H_2O_2 into the reaction medium enhances the oxidation of malachite green degradation products into smaller molecules like benzoic acid.
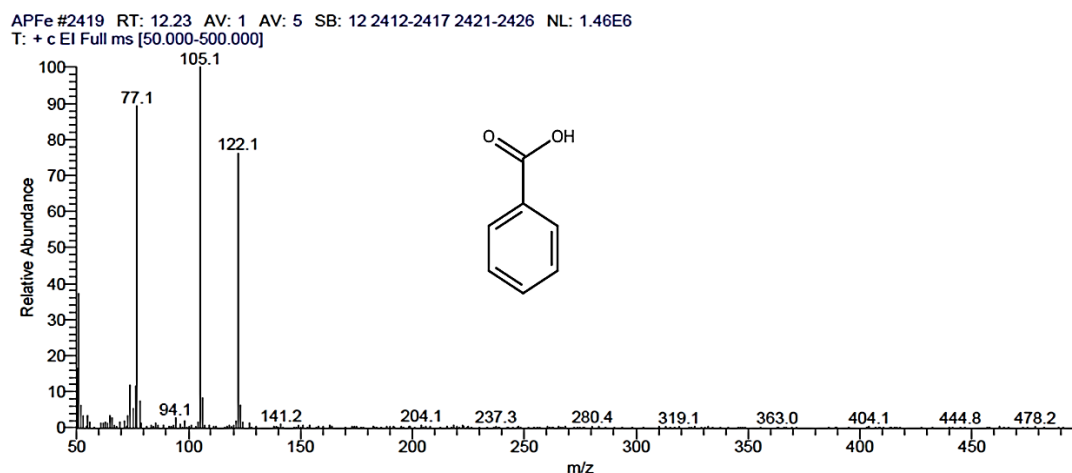
Figure 6.12 Mass spectra of benzoic acid identified by GC-MS/MS analysis
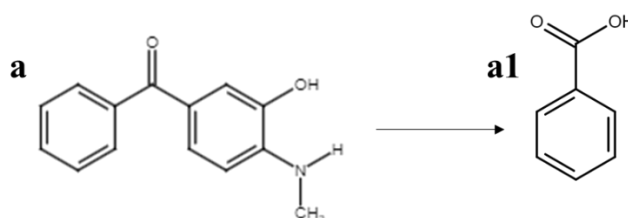
Scheme 6.1 Degradation pathway of MG using AP-Fe nanoparticles

6.4. Conclusions

The green synthesis of Fe nanoparticles using seed coat extracts of *Strychnos nux-vomica* and *Abrus precatorius* and their efficiency for removing malachite green dye and Cr(VI) has been investigated. GC-MS/MS analysis identified the bioactive components present in the AP and SN plant extracts. UV-visible spectral analysis confirms the formation of Fe nanoparticles and FTIR spectra provide the probable functional groups present in the plant component which reduces Fe^{3+} and stabilise Fe nanoparticles. AP-Fe nanoparticles have dispersed crystalline particles over an amorphous phase with particle size ranging from 3-32 nm and SN-Fe nanoparticles are amorphous with particle size ranging between 2.1-5 nm, as confirmed through HRTEM analysis. SAED pattern of the synthesised Fe nanoparticles suggests that SN-Fe nanoparticles have Fe_3O_4 composition and AP-Fe nanoparticles have a mixture of Fe^0 and Fe_3O_4 nanoparticles which is attributed to the major bioactive components present in the plant extract. Additionally, the study also envisaged that AP-Fe nanoparticles and SN-Fe nanoparticles have a high potential for the removal of Cr(VI) and MG dye. The result shows that AP-Fe nanoparticles and SN-Fe nanoparticles removed 73 % and 69 % Cr(VI) using 0.2 mL nanoparticles dosage within 15 minutes through adsorption, reduction to Cr(III) and precipitation. In the presence of H_2O_2, the prepared nanoparticles acted as Fenton-like catalyst and degraded the MG dye through oxidation. The AP-Fe and SN-Fe nanoparticles were removed 98 % and 91 % MG using 1 mL nanoparticles and H_2O_2 within 15 minutes. The parameters such as nanoparticle dosage, initial pollutant concentration, initial pH of the solution and contact time were also investigated. The study established that plant extracts can be used for the effective production of stable Fe nanoparticles, which can act as a promising source for contaminant removal.

6.5. References

[1]   Z. Xiao, M. Yuan, B. Yang, Z. Liu, J. Huang, D. Sun, Plant-mediated synthesis of highly active iron nanoparticles for Cr (VI) removal: Investigation of the leading biomolecules, Chemosphere. 150 (2016) 357–364. https://doi.org/10.1016/j.chemosphere.2016.02.056.

[2]   P.A.R. Puthukkara, T. Sunil Jose, S. Dinoop lal, Plant mediated synthesis of zero valent iron nanoparticles and its application in water treatment, J. Environ. Chem. Eng. (2020) 104569. https://doi.org/10.1016/j.jece.2020.104569.

[3]   S. Upadhyay, V.K. Dixit, A.K. Ghosh, V. Singh, Effect of petroleum ether and ethanol fractions of seeds of Abrus precatorius on androgenic alopecia, Rev. Bras. Farmacogn. 22 (2012) 359–363. https://doi.org/10.1590/S0102-695X2011005000221.

[4]   M. Biruntha, J. Archana, K. Kavitha, B. Karunai Selvi, J.A. John Paul, R. Balachandar, M. Saravanan, N. Karmegam, Green Synthesis of Zinc Sulfide Nanoparticles Using Abrus precatorius and Its Effect on Coelomic Fluid Protein Profile and Enzymatic Activity of the Earthworm, Eudrilus eugeniae, Bionanoscience. 10 (2020) 149–156. https://doi.org/10.1007/s12668-019-00694-0.

[5]   B. Gaddala, S. Nataru, Synthesis, characterization and evaluation of silver nanoparticles through leaves of Abrus precatorius L.: an important medicinal plant, Appl. Nanosci. 5 (2015) 99–104. https://doi.org/10.1007/s13204-014-0295-4.

[6]   K. Steffy, G. Shanthi, A.S. Maroky, S. Selvakumar, Potential bactericidal activity of S. nux-vomica–ZnO nanocomposite against multidrug-resistant bacterial pathogens and wound-healing properties, J. Trace Elem. Med. Biol. 50 (2018) 229–239. https://doi.org/10.1016/j.jtemb.2018.07.009.

[7]   K. Patel, D. Laloo, G.K. Singh, M. Gadewar, D.K. Patel, A review on medicinal uses, analytical techniques and pharmacological activities of Strychnos nux-vomica Linn.: A concise report, Chin. J. Integr. Med. (2017) 1–13. https://doi.org/10.1007/s11655-016-2514-1.

[8]   Q. Bin Han, S.L. Li, C.F. Qiao, J.Z. Song, Z.W. Cai, P.P.H. But, P.C. Shaw, H.X. Xu, A simple method to identify the unprocessed Strychnos seeds used in herbal medicinal products, Planta Med. 74 (2008) 458–463. https://doi.org/10.1055/s-2008-1034359.

[9]   R. Bhati, A. Singh, V. Saharan, V.A. Ram, A. Bhandari, Strychnos nux-vomica seeds: Pharmacognostical standardization, extraction, and antidiabetic activity, J. Ayurveda Integr. Med. 3 (2012) 80–84. https://doi.org/10.4103/0975-9476.96523.

[10]   K. Steffy, G. Shanthi, A.S. Maroky, S. Selvakumar, Synthesis and characterization of ZnO phytonanocomposite using Strychnos nux-vomica L. (Loganiaceae) and antimicrobial activity against multidrug-resistant bacterial strains from diabetic foot ulcer, J. Adv. Res. 9 (2018) 69–77. https://doi.org/10.1016/j.jare.2017.11.001.

[11]   T. Shahwan, S. Abu Sirriah, M. Nairat, E. Boyaci, A.E. Eroĝlu, T.B. Scott, K.R. Hallam, Green synthesis of iron nanoparticles and their application as a Fenton-like catalyst for the degradation of aqueous cationic and anionic dyes, Chem. Eng. J. 172 (2011) 258–266. https://doi.org/10.1016/j.cej.2011.05.103.

[12]   N. Garaniya, A. Bapodra, Ethno botanical and Phytophrmacological potential of Abrus precatorius L.: A review, Asian Pac. J. Trop. Biomed. 4 (2014) S27–S34. https://doi.org/10.12980/APJTB.4.2014C1069.

[13]   R. Javed, M. Zia, S. Naz, S.O. Aisida, N. ul Ain, Q. Ao, Role of capping agents in the application of nanoparticles in biomedicine and environmental remediation: recent trends and future prospects, J. Nanobiotechnology. 18 (2020) 172. https://doi.org/10.1186/s12951-020-00704-4.

[14]   R. Lakra, M.S. Kiran, P.S. Korrapati, Furfural mediated synthesis of silver nanoparticles for photocatalytic reduction of hexavalent chromium, Environ. Technol. Innov. 21 (2021) 101348. https://doi.org/10.1016/j.eti.2020.101348.

[15]   P.V. Kumar, S.M. Jelastin Kala, K.S. Prakash, Green synthesis derived Pt-nanoparticles using Xanthium strumarium leaf extract and their biological studies, J. Environ. Chem. Eng. 7 (2019) 103146. https://doi.org/10.1016/j.jece.2019.103146.

[16]   Anderson Thesing, José E. R. do Nascimento, Raquel G. Jacob, Jacqueline F. L. Santos, Eucalyptus Oil-Mediated Synthesis of Gold Nanoparticles, J. Chem. Chem. Eng. 12 (2018). https://doi.org/10.17265/1934-7375/2018.02.002.

[17]   B. Ibrahim, A. Wiranata, A. Malik, The Effect of Addition of Antioxidant 1,2-dihydro-2,2,4-trimethyl-quinoline on Characteristics of Crepe Rubber Modified Asphalt in Short Term Aging and Long Term Aging Conditions, Appl. Sci. 10 (2020) 7236. https://doi.org/10.3390/app10207236.

[18]   T. Kalaivani, C. Rajasekaran, M. Shalini, V. Vijayakumar, D.P. Pandey, L. Mathew, Structural Elucidation and Antioxidant Activity of Ethyl Gallate Isolated from Acacia nilotica (L.) Wild. ex. Delile subsp. indica (Benth.) Brenan, Natl. Acad. Sci. Lett. 41 (2018) 355–359. https://doi.org/10.1007/s40009-018-0725-z.

[19]   M. Tiwari, P. Kumar, K.K. Tejavath, V. Tiwari, Assessment of Molecular Mechanism of Gallate-Polyvinylpyrrolidone-Capped Hybrid Silver Nanoparticles against Carbapenem-Resistant Acinetobacter baumannii, ACS Omega. 5 (2020) 1206–1213. https://doi.org/10.1021/acsomega.9b03644.

[20]   A. R, R. Naika, Anti-inflammatory properties of Pavetta Crassicaulis Bremek. Leaf and flower crude extracts and its pure compounds collected from Western ghats, Karnataka, India, Asian J. Pharm. Clin. Res. 11 (2018) 72. https://doi.org/10.22159/ajpcr.2018.v11i9.21885.

[21]   W. Liang, R. Zhu, X. Li, J. Deng, Y. Fu, Heterogeneous photocatalyzed acceptorless dehydrogenation of 5-hydroxymethylfurfural upon visible-light illumination, Green Chem. 23 (2021) 6604–6613. https://doi.org/10.1039/D1GC01286J.

[22]   H. Chabane, M. Messarah, M. Liacha, Comparative study for the synthesis of new generation of 2(3H)-benzothiazolones as antioxidant agents, Der Pharma Chem. 8 (2016) 20–26.

[23]   A. Suvitha, S. Periandy, P. Gayathri, NBO, HOMO–LUMO, UV, NLO, NMR and vibrational analysis of veratrole using FT-IR, FT-Raman, FT-NMR spectra and HF–DFT computational methods, Spectrochim. Acta Part A Mol. Biomol. Spectrosc. 138 (2015) 357–369. https://doi.org/10.1016/j.saa.2014.11.011.

[24]   S.J.S. Flora, Structural, Chemical and Biological Aspects of Antioxidants for Strategies Against Metal and Metalloid Exposure, Oxid. Med. Cell. Longev. 2 (2009) 191–206. https://doi.org/10.4161/oxim.2.4.9112.

[25]   M.-B. Hu, W. Peng, Y.-J. Liu, D. Yan, X. Chen, C.-J. Wu, Maillard reaction induces changes in saccharides and amino acids during stir-baking of areca nuts, Trop. J. Pharm. Res. 15 (2016) 2107. https://doi.org/10.4314/tjpr.v15i10.8.

[26]   E.F. Seneme, D.C. dos Santos, E.M.R. Silva, Y.E.M. Franco, G.B. Longato, Pharmacological and Therapeutic Potential of Myristicin: A Literature Review, Molecules. 26 (2021) 5914. https://doi.org/10.3390/molecules26195914.

[27]   K. Abdulwahab, M.A. Malik, P. O'Brien, K. Govender, C.A. Muryn, G.A. Timco, F. Tuna, R.E.P. Winpenny, Synthesis of monodispersed magnetite nanoparticles from iron pivalate clusters, Dalt. Trans. 42 (2013) 196–206. https://doi.org/10.1039/C2DT32478D.

[28]   A. Rana, N. Kumari, M. Tyagi, S. Jagadevan, Leaf-extract mediated zero-valent iron for oxidation of Arsenic (III): Preparation, characterization and kinetics, Chem. Eng. J. 347 (2018) 91–100. https://doi.org/10.1016/j.cej.2018.04.075.

[29]   Z. Xiao, H. Zhang, Y. Xu, M. Yuan, X. Jing, J. Huang, Q. Li, D. Sun, Ultra-efficient removal of chromium from aqueous medium by biogenic iron based nanoparticles, Sep. Purif. Technol. 174 (2017) 466–473. https://doi.org/10.1016/j.seppur.2016.10.047.

[30]   D. Patiño-Ruiz, L. Sánchez-Botero, L. Tejeda-Benitez, J. Hinestroza, A. Herrera, Green synthesis of iron oxide nanoparticles using Cymbopogon citratus extract and sodium

carbonate salt: Nanotoxicological considerations for potential environmental applications, Environ. Nanotechnology, Monit. Manag. 14 (2020) 100377. https://doi.org/10.1016/j.enmm.2020.100377.

[31] P. Prema, S. Thangapandian, M. Selvarani, S. Subharanjani, C. Amutha, Color removal efficiency of dyes using nanozerovalent iron treatment, Toxicol. Environ. Chem. 93 (2011) 1908–1917. https://doi.org/10.1080/02772248.2011.606613.

[32] C. Prasad, K. Sreenivasulu, S. Gangadhara, P. Venkateswarlu, Bio inspired green synthesis of Ni/Fe3O4 magnetic nanoparticles using Moringa oleifera leaves extract: A magnetically recoverable catalyst for organic dye degradation in aqueous solution, J. Alloys Compd. 700 (2017) 252–258. https://doi.org/10.1016/j.jallcom.2016.12.363.

[33] K.V.G. Ravikumar, S.V. Sudakaran, K. Ravichandran, M. Pulimi, C. Natarajan, A. Mukherjee, Green synthesis of NiFe nano particles using Punica granatum peel extract for tetracycline removal, J. Clean. Prod. 210 (2019) 767–776. https://doi.org/10.1016/j.jclepro.2018.11.108.

[34] E.S. Madivoli, P.G. Kareru, A.N. Gachanja, S.M. Mugo, D.S. Makhanu, Phytofabrication of iron nanoparticles and their catalytic activity, SN Appl. Sci. 1 (2019). https://doi.org/10.1007/s42452-019-0951-0.

[35] S. Eslami, M.A. Ebrahimzadeh, P. Biparva, Green synthesis of safe zero valent iron nanoparticles by: Myrtus communis leaf extract as an effective agent for reducing excessive iron in iron-overloaded mice, a thalassemia model, RSC Adv. 8 (2018) 26144–26155. https://doi.org/10.1039/c8ra04451a.

[36] Y. Wei, Z. Fang, L. Zheng, E.P. Tsang, Biosynthesized iron nanoparticles in aqueous extracts of Eichhornia crassipes and its mechanism in the hexavalent chromium removal, Appl. Surf. Sci. 399 (2017) 322–329. https://doi.org/10.1016/j.apsusc.2016.12.090.

[37] F. Zhu, S. He, T. Liu, Effect of pH, temperature and co-existing anions on the Removal of Cr(VI) in groundwater by green synthesized nZVI/Ni, Ecotoxicol. Environ. Saf. 163 (2018) 544–550. https://doi.org/10.1016/j.ecoenv.2018.07.082.

[38] F. Zhu, S. Ma, T. Liu, X. Deng, Green synthesis of nano zero-valent iron/Cu by green tea to remove hexavalent chromium from groundwater, J. Clean. Prod. 174 (2018) 184–190. https://doi.org/10.1016/j.jclepro.2017.10.302.

[39] A. Soliemanzadeh, M. Fekri, The application of green tea extract to prepare bentonite-supported nanoscale zero-valent iron and its performance on removal of Cr(VI): Effect of relative parameters and soil experiments, Microporous Mesoporous Mater. 239 (2017) 60–69. https://doi.org/10.1016/j.micromeso.2016.09.050.

[40] X. Jin, Y. Liu, J. Tan, G. Owens, Z. Chen, Removal of Cr(VI) from aqueous solutions via reduction and absorption by green synthesized iron nanoparticles, J. Clean. Prod. 176 (2018) 929–936. https://doi.org/10.1016/j.jclepro.2017.12.026.

[41] P.V. Nidheesh, R. Gandhimathi, S.T. Ramesh, Degradation of dyes from aqueous solution by Fenton processes: A review, Environ. Sci. Pollut. Res. 20 (2013) 2099–2132. https://doi.org/10.1007/s11356-012-1385-z.

[42] X. Wang, A. Wang, J. Ma, M. Fu, Facile green synthesis of functional nanoscale zero-valent iron and studies of its activity toward ultrasound-enhanced decolorization of cationic dyes, Chemosphere. 166 (2017) 80–88. https://doi.org/10.1016/j.chemosphere.2016.09.056.

[43] P. Anju Rose Puthukkara, T. Sunil Jose, S. Dinoop lal, A.R. Puthukkara P, S. Jose T, D. lal S, Chitosan stabilized Fe/Ni bimetallic nanoparticles for the removal of cationic and anionic

triphenylmethane dyes from water, Environ. Nanotechnology, Monit. Manag. 14 (2020) 100295. https://doi.org/10.1016/j.enmm.2020.100295.

[44]   L. Huang, X. Weng, Z. Chen, M. Megharaj, R. Naidu, Green synthesis of iron nanoparticles by various tea extracts: Comparative study of the reactivity, Spectrochim. Acta - Part A Mol. Biomol. Spectrosc. 130 (2014) 295–301. https://doi.org/10.1016/j.saa.2014.04.037.

[45]   G. Sharma, S. Bhogal, V.K. Gupta, S. Agarwal, A. Kumar, D. Pathania, G.T. Mola, F.J. Stadler, Algal biochar reinforced trimetallic nanocomposite as adsorptional/photocatalyst for remediation of malachite green from aqueous medium, J. Mol. Liq. 275 (2019) 499–509. https://doi.org/10.1016/j.molliq.2018.11.070.